Discrete stochastic charging of aggregate grains

Lorin S. Matthews, Babak Shotorban, and Truell W. Hyde

Discrete stochastic charging of aggregate grains

Lorin S. Matthews[1], Babak Shotorban[2], and Truell W. Hyde[1]

[1] *Center for Astrophysics, Space Physics, and Engineering Research One Bear Place 97310, Waco, TX 76798*
[2] *Department of Mechanical and Aerospace Engineering, The University of Alabama in Huntsville, Huntsville, AL 35899*

Abstract

Dust particles immersed in a plasma environment become charged through the collection of electrons and ions at random times, causing the dust charge to fluctuate about an equilibrium value. Small grains (with radii less than 1 μm) or grains in a tenuous plasma environment are sensitive to single additions of electrons or ions. Here we present a numerical model that allows examination of discrete stochastic charge fluctuations on the surface of aggregate grains and determines the effect of these fluctuations on the dynamics of grain aggregation. We show that the mean and standard deviation of charge on aggregate grains follows the same trends as those predicted for spheres having an equivalent radius, though aggregates exhibit larger variations from the predicted values. In some plasma environments, these charge fluctuations occur on timescales which are relevant for dynamics of aggregate growth. Coupled dynamics and charging models show that charge fluctuations tend to produce aggregates which are much more linear or filamentary than aggregates formed in an environment where the charge is stationary.

I. INTRODUCTION

One of the fundamental processes which occurs in a complex plasma environment is the charging of dust grains, nm – mm-sized solid particulates immersed in the plasma. Dust particles acquire charge through direct collisions with electrons and ions, and in most cases will become negatively charged due to the initial large flux of electrons to the uncharged grain. In some plasma environments, secondary electron emission (SEE) or photoemission can contribute to the charging process, and dust grains can become positively charged.

The charge on the grains is gained or lost in discrete units of elementary charge at random time intervals, with the charge on a grain fluctuating about the average equilibrium charge. It was predicted theoretically [1], and later confirmed through numerical simulations of the fluctuations [2], [3] and solutions to master or Fokker-Plank (FP) equations [4]–[7] that the time-averaged charge on the grain is linearly proportional to the grain radius, while the standard deviation is proportional to the square root of the average charge. Thus, the magnitude of the charge fluctuations relative to the equilibrium charge decreases as the grain size increases.

For example, under typical experimental conditions using a RF plasma, grains collect ~1,000 elementary charges per micron of radius, with a charge fluctuation on the order of 1% of the equilibrium charge [4]. However, in cases where the grain size is small, the plasma is cold or tenuous, or the dust density is large enough to remove a significant fraction of the electrons from the plasma, the average charge can be as small as hundreds or even tens of electrons. In this case, charge fluctuations can become

a significant fraction of the equilibrium charge [4]. At the same time, the characteristic time scale for these charge fluctuations can become comparable to the time scales of the dynamic processes affecting the dust [3], [5].

A particular case where discrete stochastic charge (DSC) fluctuations can play a role in the dynamic response of the dust grains is the growth of the dust through aggregation. In the low pressure plasmas used for etching or chemical-vapor deposition, the formation and growth of fine particles can be detrimental to the system [8], although a similar process is often utilized to study the nucleation and growth process [9], [10]. The production of ultrafine powders with prescribed size ranges also takes advantage of thermal nucleation and particle charging, such as the nanoparticles produced for use in inhalation toxicity studies [11]. In protoplanetary disks, aggregate growth from small particles is a necessary preliminary step in the formation of the larger bodies which eventually form planetary systems. In each of the above, charge fluctuations can affect the coagulation rate, aggregate porosity, and maximum grain size [12]. In some environments, fluctuating charge on very small grains can even allow them to become positively charged [2], [3] leading to oppositely charged grains in the overall population and sometimes creating runaway growth [13], [14].

Our previous work on stochastic charging extended the stochastic charging model to non-spherical aggregate grains by treating charge as a continuous variable with charging time steps set as a fixed fraction of the equilibrium charging time [12]. As noted above, however, in many cases the grain charge is small enough that the gain or loss of charge should be quantized in units of the elementary charge, which also requires predicting the (random) elapsed time for the addition of a charged particle. In this study, a methodology is developed to model discrete fluctuations over the surface of an irregular dust grain, with the addition of electrons and ions occurring at random times at random locations on the dust surface.

The paper is organized as follows: Section 2 provides an overview of the charging currents calculated from OML theory, and describes how these currents are used to calculate the electron and ion currents to points on a grain surface. Section 3 describes how the currents to the surface points are used to calculate the stochastic variation of the charge, by determining the random elapsed time, the charge (electron or ion) to be added and the location on the grain surface for the addition. As shown in Section 4, the model is validated by applying it to spherical grains and comparing the results to those found from previous models which treat the grain surface as an isopotential. The discrete stochastic charging method is then applied to aggregate grains to examine the time scale of the fluctuations. Finally, a dynamic model of collisional grain growth including the effects of stochastic charge variations is presented in Section 5 to illustrate the effects of these fluctuations on aggregate grain growth.

II. CHARGING CURRENTS

In this paper, we limit our analysis to grain charging through collisional currents of primary electron and ion to the dust surface. This method can easily be extended to include secondary charging effects such as photoemission and secondary electron emission [15]. Inherent assumptions we make in the following are that the particle radius is smaller than the Debye length of the plasma, which is smaller than the mean free path of the plasma particles, $a \ll \lambda_D \ll \lambda_{mfp}$, and that the interparticle distance between dust grains is larger than the Debye length, such that the charge on a grain is independent of other grains.

A. OML charging currents

The charge on a dust particle is commonly determined using orbital-motion-limited theory to find the primary electron and ion currents to the grain as a function of the grain potential [16]. The current density J_s to a point on the surface of a grain is determined by the flux of particles with enough energy to overcome the coulomb potential barrier to reach the surface

$$J_s = q_s n_s \int_{v_{min}}^{\infty} v_s^3 f(v_s) \sigma(v_s) \, dv_s \iint \cos\gamma \, d\Omega \qquad (1)$$

where n_s is the plasma density of species s (electron or ion) very far from the grain, q_s the charge of the incoming plasma particle of mass m_s and temperature T_s, v_s the velocity of the incoming plasma particle with a velocity distribution $f(v_s)$, and $\sigma(v_s)$ the effective cross section of the charged target [16], which is $\sigma(v_s) = \left(1 - 2q_s\phi_d/m_s v_s^2\right)$ for particles with $2q_s\phi_d/mv_s^2 \leq 1$ and zero otherwise. The lower limit of integration for the particle velocity is the minimum velocity required for a charged plasma particle to reach a point on the surface of a dust grain having potential ϕ_d. Thus, the minimum velocity is either zero, when the plasma species and dust have opposite charge, or $v_{min} = \sqrt{2q_s\phi_d/m_s}$, for plasma species and dust of the same charge polarity. In the integration over the angles, γ is the angle between the velocity vector and the surface normal, and $d\Omega = \sin\theta d\theta d\phi$ the solid angle from which the plasma particle approaches the surface. Assuming that the electrons and ions have Maxwellian velocity distributions characterized by the temperatures T_e and T_i, respectively, Eq. 1 can be integrated easily for a point on the surface of a spherical grain. The current to the grain surface is then found by multiplying the current density by the surface area, yielding

$$I_s = I_{0s} \exp\left(-\frac{q_s\phi_d}{kT_s}\right) \quad q_s\phi_d > 0$$

$$\qquad (2)$$

$$I_s = I_{0s}\left(1 - \frac{q_s\phi_d}{kT_s}\right) \qquad q_s\phi_d < 0$$

The coefficient I_{0s} represents the currents to an uncharged grain of radius a; assuming the plasma is isotropic and not flowing past the grain, this is

$$I_{0s} = 4\pi a^2 n_s q_s \left(\frac{kT_s}{2\pi m_s}\right)^{1/2} \qquad (3)$$

Initially, the electron current to an uncharged grain is greater than the ion current. As the grain accumulates negative charge, slower moving electrons will not have the energy required to reach the grain surface, while ions continue to be attracted to the grain. Eventually an equilibrium potential is reached when the electron and ion currents are equal, where ϕ_d is the solution to

$$\exp\left(\frac{e\phi_d}{kT_e}\right) = \frac{n_e}{n_i}\left(\frac{m_e T_i}{m_i T_e}\right)^{1/2}\left(1 - \frac{e\phi_d}{kT_i}\right). \qquad (4)$$

The equilibrium charge on a spherical grain is then given by

$$Q = 4\pi\varepsilon_0 a\phi_d. \qquad (5)$$

B. OML_LOS: Charging of non-spherical grains

Non-spherical grains, such as aggregates comprised of spherical monomers, have a varying surface potential. (This can be true for a spherical dielectric grain as well, if the rate of collection of electrons and ions is fast compared to the time scale for charge recombination on the surface, but not so fast as to keep all points on the surface in equilibrium.) In addition to the varying potential, the trajectories of incoming plasma particles to some points on the surface may also be blocked by other monomers in the aggregate. OML theory requires that all positive energy orbits connect back to infinity, and not originate from another point on the grain [17]. To numerically integrate the flux given in Eq. 1, the surface is divided into patches surrounding points which are uniformly distributed over the surface of each sphere (see Fig. 1) [18]. It is assumed that an elementary charge (ion or electron) that arrives at the particle surface stays at the point of impact.
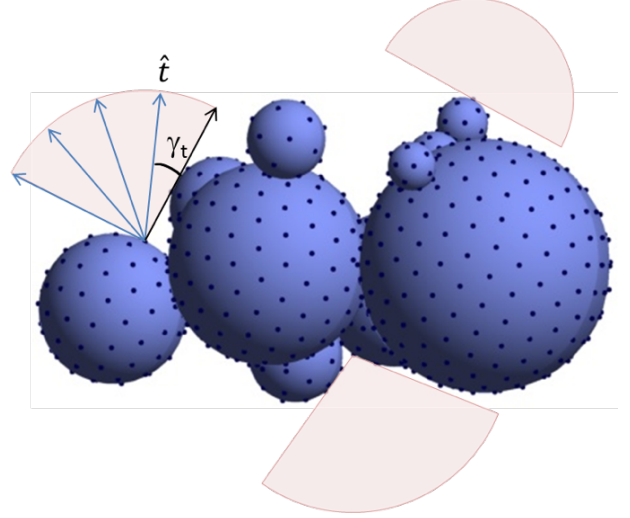

FIG. 1. A 2D representation of the open lines of sight to three points on the surface of an aggregate. The open lines of sight are determined by checking many test directions $\hat{t}$ to see if they intersect other monomers in the aggregate. The angle between the surface normal vector and the test direction is γ_t.

The potential at the center of each patch ϕ_p is calculated from the charge q_j on all other surface points (at distance r_{pj} away) and the patch itself, $\phi_p = \sum_j q_j / r_{pj} + \phi_c$. The potential at the center of the patch, $\phi_c = q_p \sqrt{2/(1-\cos\theta)}/4\pi\varepsilon_0 a$, is approximated by the potential at the center of a spherical cap with surface charge density $\sigma = q_p/2\pi a^2(1-\cos\theta)$, where θ is equal to the average angular separation between the points. As each patch on the surface of a sphere is actually a polygon, the accuracy of this approximation increases with the number of patches used in the simulation.

The current density incident on each patch is determined by numerical integration of Equation 1. The integral over the speed v_s is exact, and can be calculated once the potential ϕ_p is known. The integral over the angles is approximated by breaking up the solid angle into many sections characterized by test directions $\hat{t}$ and determining which lines of sight (LOS) are blocked by other monomers in the aggregate, as illustrated in Figure 1. The LOS factor $LOS_p = \iint \cos\gamma \, d\Omega \approx \sum_t \cos\gamma_t \, \Delta\Omega$, is obtained by summing over the open LOS (see Matthews et al. [18] for a complete description of this treatment). The electron and ion currents to a patch are then the same as those given by Eq. 2 with I_{0s} replaced by the coefficient

$$I'_{0s} = A_p n_s q_s \left(\frac{kT_s}{2\pi m_s} \right)^{1/2} LOS_p / \pi \qquad (6)$$

where A_p is the area of the patch.

III. DISCRETE STOCHASTIC CHARGING METHOD

The electrons and ions in the plasma do not constitute a continuous fluid, but rather individually reach the grain surface at random times. The Fokker-Planck equation for stochastic charging of aggregates developed by Matthews et al [12] treated the charge as a continuous variable, but here the charging model developed here allows for integer increments of elementary charges collected on the surface patches.

As described in [12], a generalized form of the master equation given by Matsoukas and Russell [4], [5] and Shotorban [6] can be formulated to determine the charge collected on each patch, and hence the entire surface of the grain, utilizing the ion and electron currents to each patch. The set of elementary charges collected on the patches is defined by the vector $\mathbf{Z} = \{Z_1, Z_2, ..., Z_n\} \in \mathbb{R}^n$, where there are n patches on the aggregate, (e.g., Z_2 is the number of elementary charges collected on the patch number 2). Assuming that $\mathbf{Z}$ undergoes a Markov process [19], the master equation is

$$\frac{dP(\mathbf{Z},t)}{dt} = \sum_{p=1}^{n} I_{i,p}(\mathbf{Z} - \mathbf{e}_p)P(\mathbf{Z} - \mathbf{e}_p, t) + I_{e,p}(\mathbf{Z} + \mathbf{e}_p)P(\mathbf{Z} + \mathbf{e}_p, t) - [I_{i,p}(\mathbf{Z}) + I_{e,p}(\mathbf{Z})]P(\mathbf{Z},t) \qquad (7)$$

where $P(\mathbf{Z}, t)$ is the joint probability density function. In this equation, $I_{e,p}$ and $I_{i,p}$ are the electron and ion attachment *rates* (i.e., the electron and ion currents divided by the charge), to patch p, and $\mathbf{e}_p \in \mathbb{R}^n$ is the unit vector, e. g., $\mathbf{e}_3 = \{0, 0, 1, ... , 0\}$. It is assumed no charge is transferred from one patch to another.

In accordance with the master equation, the discrete stochastic method (DSM) is based on the following algorithm, which is a customized version of the stochastic simulation algorithm developed for chemical kinetics [20], [21], to calculate discrete charge fluctuations on patches. The system is initialized with the charges of patches set to $\mathbf{Z} = \mathbf{Z}_0$ at $t = t_0$, where $\mathbf{Z}_0$ is the initial condition. The attachment rates, $I_{i,p}(\mathbf{Z})$ and $I_{e,p}(\mathbf{Z})$, are found from the currents to each patch (Equation (6)), and then used to calculate the sum of the attachment rates to all patches,

$$\lambda(\mathbf{Z}) = \sum_{p=1}^{n} I_{i,p}(\mathbf{Z}) + I_{e,p}(\mathbf{Z}) \qquad (8)$$

Then, a random number r_1 is generated from a uniform distribution with $0 \leq r_1 \leq 1$ and used to determine the time interval τ which elapses before the attachment of the next plasma particle

$$\tau = \frac{1}{\lambda(\mathbf{Z})} \ln\left(\frac{1}{r_1} \right) \qquad (9)$$

The type of the plasma particle and the patch p to which the particle is attached is determined by generating a second random number, r_2, and finding k, the smallest integer satisfying

$$\sum_{k'=1}^{k} I_{k'}(Z) > r_2 \lambda(\mathbf{Z}) \qquad (10)$$

where we have defined

$$I_{k'}(\mathbf{Z}) = \begin{cases} I_{i,p}(\mathbf{Z}) \text{ if } k' = 2p-1 \\ I_{e,p}(\mathbf{Z}) \text{ if } k' = 2p \end{cases} \qquad (11)$$

If k is odd, then the attached particle is an ion and the patch to which the particle is attached is $p = (k+1)/2$. If k is even, then the attached particle is an electron and the patch is $p = k/2$. Following this notation, for instance, $I_7(\mathbf{Z}) = I_{i,4}(\mathbf{Z})$ is the ion current to patch number 4 and $I_8(\mathbf{Z}) = I_{e,4}(\mathbf{Z})$ is the electron current to patch number 4. The time is then updated from t to $t+\tau$, and the charge is updated from $\mathbf{Z}$ to $\mathbf{Z} + \mathbf{e}_p$ if the attached particle is an ion, or $\mathbf{Z}$ to $\mathbf{Z} - \mathbf{e}_p$ if the attached particle is an electron. The procedure is iterated until the desired length of time has elapsed.

The charge on a grain fluctuates about the mean charge $\langle Z \rangle$, as expressed in Eq. 5, with the variance of the charge state given by [5]

$$\sigma^2 = 4\pi\varepsilon_0 a k_B T_e \left(1 - \frac{1}{1 + T_i/T_e - e\phi_d/k_B T_e} \right). \qquad (12)$$

IV. CHARGING WITH THE DSM

In the following section we compare the DSM for calculation of charge collected on patches on the surface of a grain to previous studies which modeled the stochastic fluctuation of charge on spherical grains [3], [5].

We apply the model using two different plasma conditions, the first being a typical low-temperature plasma discharge environment with the second using conditions which may be found in an astrophysical plasma such as that found in a protoplanetary disk (PPD). The two plasma environments will be referred to as *LAB plasma* and *PPD plasma*, respectively. Conditions for the LAB plasma assume singly ionized argon with electron and ion temperatures $T_e = 1$ eV, $T_i = 500$ K, and equal electron and ion number densities, $n_e = n_i = 10^{16}$ m^{-3} [5]. The condition for the PPD plasma are chosen to represent a region of the disk where the dust density is large enough to deplete the electrons in the plasma [12], [18]. The ionized species is considered to be hydrogen with $T_e = T_i = 900$ K, ion density $n_i = 5 \times 10^8$ m^{-3}, and electron density $n_e = 0.1 n_i$.

We first show that the discrete stochastic charging method recovers the results previously reported for stochastic fluctuations on charge on spherical grains and then apply the DSM to the charging of aggregates consisting of spherical monomers.

A. Validation of DSM: Spherical Grains

Charging simulations were carried out for spheres with radii $a = 10, 20, 50, 100, 200, 500,$ and 1000 nm, and varying number of patches on the surface with $n = 10, 20, 40,$ and 90. The simulations included 100,000 time steps determined by eq. (9). Sample charging histories and probability distributions of the fluctuating charge are shown in Figure 2 for a 20 nm grain in a LAB plasma and a 100 nm grain in a PPD plasma.
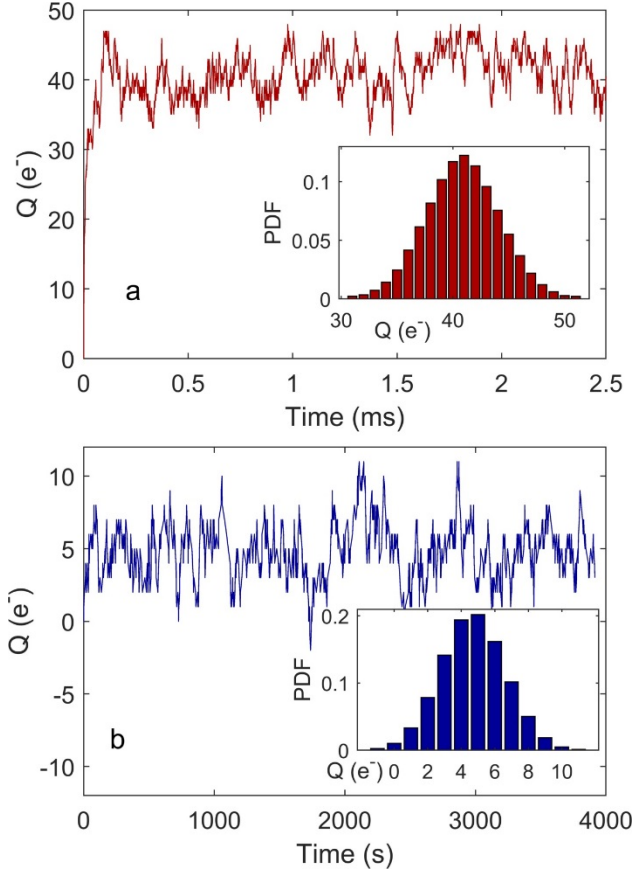
FIG. 2. First 2500 time steps of the charging history and (insets) probability distribution of the fluctuating charge (for 70,000 time steps after equilibrium is reached). a) 20 nm grain with resolution $n = 20$ in LAB plasma conditions, b) 100 nm grain with resolution $n = 10$ in a PPD plasma.
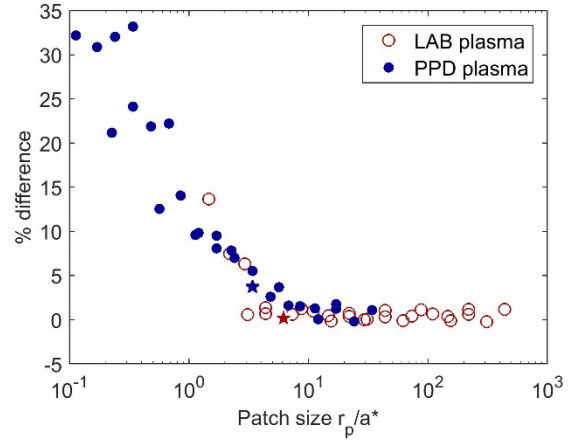
FIG. 3. Percent difference between the equilibrium charge calculated with DSC and the predicted value as a function of the patch size. Points are shown for grain radii ranging from 10 nm to 1 μm using resolutions of 10, 20, 40, and 90 surface patches. The two grains shown in Figure 2 are marked with stars.

The master equation in the DSM assumes attachment rates vary linearly with charge. This condition is automatically satisfied for the ion current to a negatively charged grain, but the electron current to a negative grain varies exponentially with the potential (and hence the charge). This linearity criterion is satisfied by requiring a minimum grain radius for given plasma parameters, $a* = e^2 / (4\pi \acute{U}_0 k_b T_e)$, as noted in [5]. Here we apply this as a criterion for the minimum patch size. Taking the area of a patch to be $A_p = 4\pi a^2/n$, the radius of a patch r_p can be estimated from $A_p = \pi r_p^2$, so that the number of patches $n = (2a/r_p)^2$. The linearity criterion is well satisfied if $r_p > 10a*$ such that the maximum number of patches can be set by $n_{max} = (2a/10a*)^2$. The effect of changing the number of patches used in calculating the charge is shown in Figure 3 for several different particle radii using the two different plasma conditions, where $a^* = 1.5$ nm for the LAB plasma and $a^* = 19$ nm for the PPD plasma. The average charge on each sphere (averaged over the last 70,000 time steps) differs from the charge predicted for a

sphere (Eq. 5) by less than 2%, for $r_p > 7a*$, as shown in Figure 3. Patch sizes comparable to $a*$ still produce reasonable results, with the average charge over-predicted by 10-15%.

One of the main characteristics of the charge fluctuations on spherical grains is that the time scale of the fluctuations depends on the grain size, with small grains expriencing longer fluctuation times than larger grains in the same plasma environment [3], [5]. Figure 4 shows the growth and dissipation times for fluctuations of different magnitude for a 20 nm grain (LAB plasma) and a 100 nm grain (PPD plasma), calculated from the time history of the charge. The lines are analytic fits for the first-passage problem, as given by Matsoukas and Russell [5]

$$t_g(\Delta Q) = \tau_f \left[\sqrt{\pi/2} \int_0^{|\Delta Q|/\sigma} e^{x^2/2} erf\left(x/\sqrt{2}\right) dx \right] , \quad (13)$$

$$t_d(\Delta Q) = \tau_f \left[\sqrt{\pi/2} \int_0^{|\Delta Q|/\sigma} e^{x^2/2} erfc\left(x/\sqrt{2}\right) dx \right]. \quad (14)$$

The characteristic fluctuation time τ_f is approximately equal to the point where the growth and dissipation curves cross, and can be calculated from
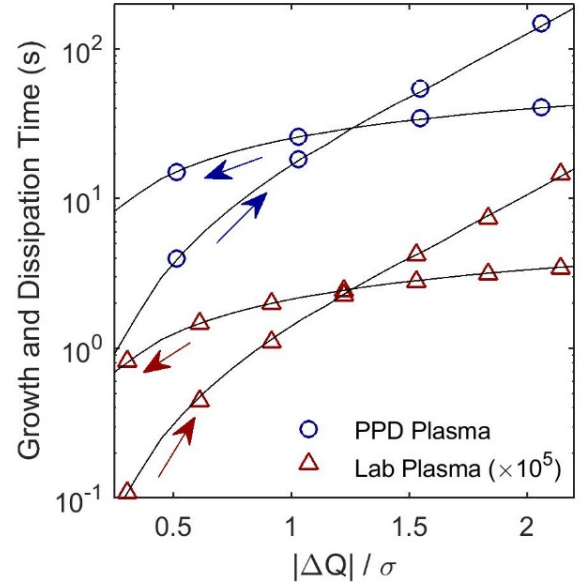

FIG. 4. Characteristic times for growth (right arrows) and dissipation (left arrows) of fluctuations. The symbols are calculated from the charging time history of a 20 nm grain in a LAB plasma and a 100 nm grain in a PPD plasma. The lines are analytic results for a sphere.

$$\tau_f = \left(\frac{4\lambda^2_i}{v_i a}\right) \frac{1}{1 + T_i/T_e - e\phi_d/k_B T_e} \quad (13)$$

where $\lambda_i = \left(\epsilon_0 k_B T_i / n_i e^2\right)^{1/2}$ is the ion Debye length and $v_i = \left(8k_B T_i / \pi m_i\right)^{1/2}$ is the average speed of the ions.

The excellent agreement between the analytic solutions for mean grain charge (Fig. 3) and fluctuation times (Fig. 4) demonstrate that the patch model is a valid technique for calculating the fluctuating grain charge.

B. Application of the DSM to Aggregates

Having verified the accuracy of DSM for a sphere, this methodology is applied to aggregates of spherical grains. We test the method using three different populations of aggregates built by ballistic particle-cluster aggregation of 1) monodisperse 500 nm spheres ($n = 20$ patches), 2) monodisperse 1.0 micron spehres ($n = 40$ patches), and 3) polydisperse spheres with monomer radii 0.5 μm $\le$ a $\le$ 10 μm with a size distribution typical of astrophysical environments, $n(a)da = a^{-3.5}da$. The number of patches used in the polydisperse case varied from $n = 10$ to $n = 1000$, depending on the monomer surface area. In
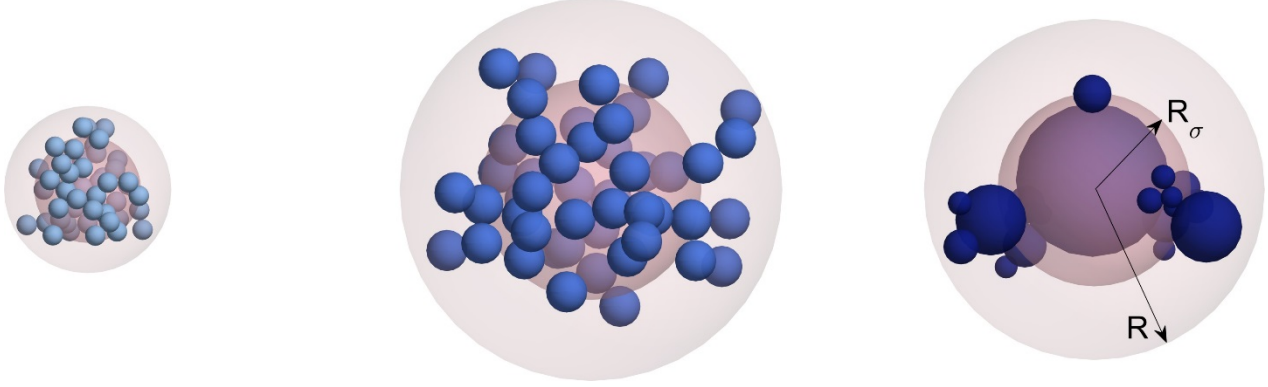
FIG. 5. Sample aggregates from the three populations, shown to scale. (Left) Aggregates with monomer radius $a = 500$ nm, (Center) aggregates with monomer radius $a = 1\,\mu$m, (Right) aggreagates with monomer radii ranging from 0.5 to 10 μm. Superimposed on each aggregate is a sphere with radius equal to R_σ, as described in the text, and a sphere with radius R (centered at the aggregate's center of mass) which just circumscribes the aggregate.

all cases the patch size was greater than $10r*$, as established above. Sample aggregates from the three populations are shown in Fig. 5. The results for the aggregates are compared to those for spherical particles with radii ranging from 0.5 to 10 μm ($n = 20$ surface patches).

As the charge and standard deviation are shown to be proportional to a particle's radius (Eqs. 5 and 12), here we define an equivalent radius for the aggregates, R_σ, which is calculated from an aggregate's projected cross section averaged over many orientations [22]. The equivalent radius has shown to be a good measure of the effective particle size, with the charge on aggregate grains varying linearly with R_σ [18]. The equivalent radius is also used to define the compactness parameter, $\Phi_\sigma = \sum_i a_i^3/R_\sigma^3$, which is used characterize the aggregate structure and determine drag forces and collision cross sections in dynamical simulations.

The charge and standard deviation shown for aggregate grains follow the same trends as for spherical grains. For illustrative purposes, we present the results calculated for PPD plasma conditions. The average charge and standard deviation, calculated over 90,000 time steps using PPD plasma conditions, are shown in Figure 6a and 6b for spheres (filled circles) and aggregates of spherical monomers (open circles). The average charge is proportional to the equivalent radius R_σ in agreement with Eq. 5, though aggregates collect a greater charge than spherical grains due to their increased surface area (Figure 6a). The inset shows the charge normalized by the predicted charge on a sphere with $R = R_\sigma$. It is evident that the difference is greatest for aggregates comprised of smaller monomers, as these aggregates tend to have the greatest surface area. The standard deviation in the charge as a fraction of the predicted charge $Q_0 = 4\pi \dot{U} R_\sigma \phi_d$, shown in Fig. 6b, is inversely proportional to the particle radius, as the fluctuations become comparatively smaller as the equilibrium charge increases. However, comparing the standard deviation to that predicted for an equivalent sphere (Eq. 12) shows that there is wide variation in σ and that the deviation is more likely to be greater than that predicted by theory (Fig. 6b inset).

The effect of the increased charge can be seen in the fluctuation times measured for the aggregates. Growth and dissipation curves for aggregate grains in the two different plasma conditions are shown in Figure 7a, along with the curves predicted for an equivalent spherical grain with radius equal to R_σ. In both cases, the growth and dissipation curves for the aggregates lie well below the predicted values. The predicted fluctuation times τ_f calculated using the aggregate equivalent radius (Eq. 12) are compared to the fluctuation times τ_c calculated from the intersection of the growth and dissipation curves in Fig 7b. It is interesting to note that though the charge on aggregate grains may be increased by as much as 20%

compared to the charge on spherical grains, the calculated fluctuation times tend to be shorter by a factor of ~3 and may differ by nearly a factor of ten. This is significant because the timescale of fluctuations on small grains may then become comparable to the time scale on which particles approach and collide with each other, affecting their collision dynamics.
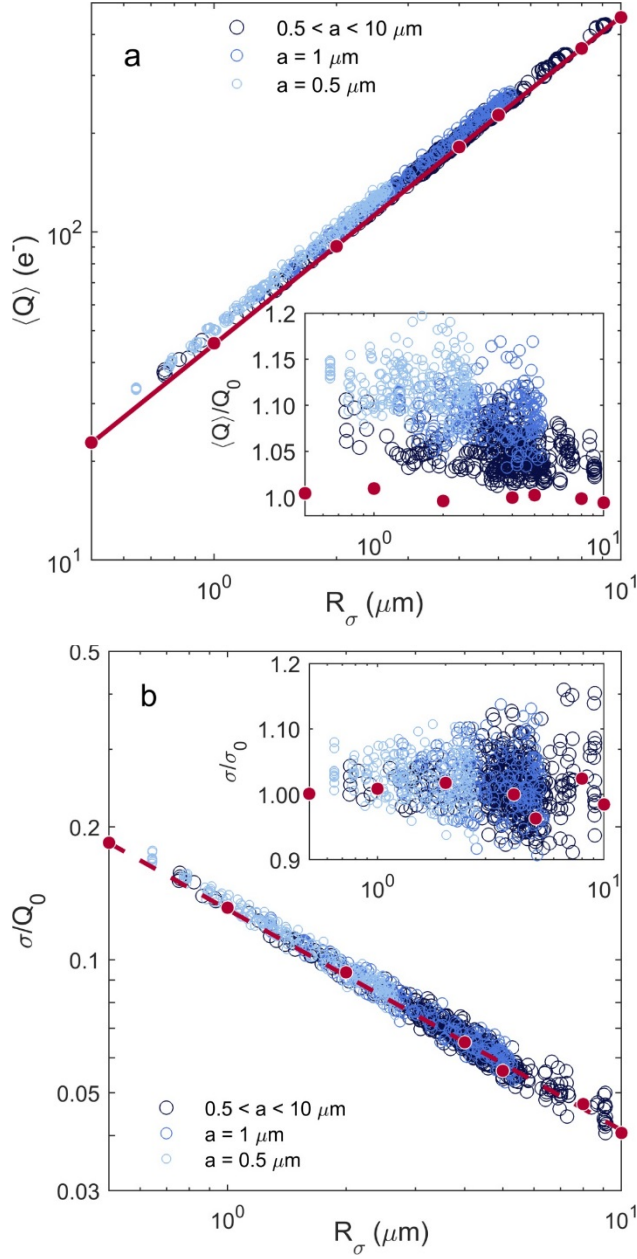
FIG. 6. Average charge (a) and standard deviation of charge as a fraction of the predicted charge (b) for aggregates of spherical monomers with radius a, as indicated in the legend. Data calculated for spheres using the DSM are shown by filled circles. The lines in (a) and (b) are theoretical predictions for spherical grains, and insets show the charge mean and standard deviation normalized by the predicted values. All data shown above were generated for PPD plasma conditions.
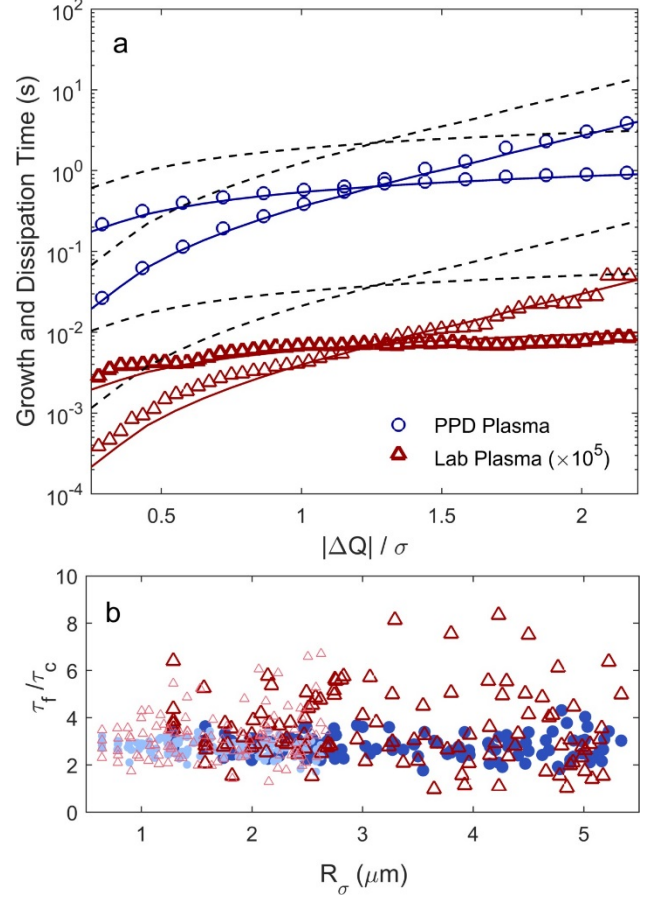

FIG. 7. (Color online) a) Characteristic times for growth and dissipation of charge fluctuations on aggregate grains consisting of 10 monomers with radius $a = 500$ nm. The dashed lines are analytic results using τ_i calculated for an equivalent sphere, while the solid lines are from the analytic fits using τ_c determined from the point where the growth and dissipation curves intersect. b) Ratio of predicted and calculated fluctuation timescales for aggregates in LAB plasma conditions (red, open symbols) and PPD plasma conditions (blue, filled symbols). The larger, darker symbols are for aggregates with $a = 1$ μm; smaller, lighter symbols are for aggregates with $a = 500$ nm.

V. EFFECTS OF DSC FLUCTUATIONS ON DYNAMICS AND AGGREGATION

The primary difference between our method and previous methods, which treated discrete fluctuations of charge on a spherical grain, is the asymmetry in the electrostatic potential. The deviation from spherical shells of constant potential can be quite significant, resulting in a strong non-uniformity on the charge distribution on the surface of the sphere. Figure 8a shows the contour lines for a 100 nm grain with five electrons on its surface, charged in PPD plasma conditions yielding an average grain charge of 4.7 e⁻. While the resolution used is $n = 10$ patches, only five of the patches carry a charge. A similar plot is shown for the same 100-nm grain under LAB plasma conditions where the average grain charge is 214 e⁻ (Fig. 8b). In this case the charge on each patch ranges from 15 e⁻ to 30 e⁻, and the deviation from circular contour lines is much less pronounced.
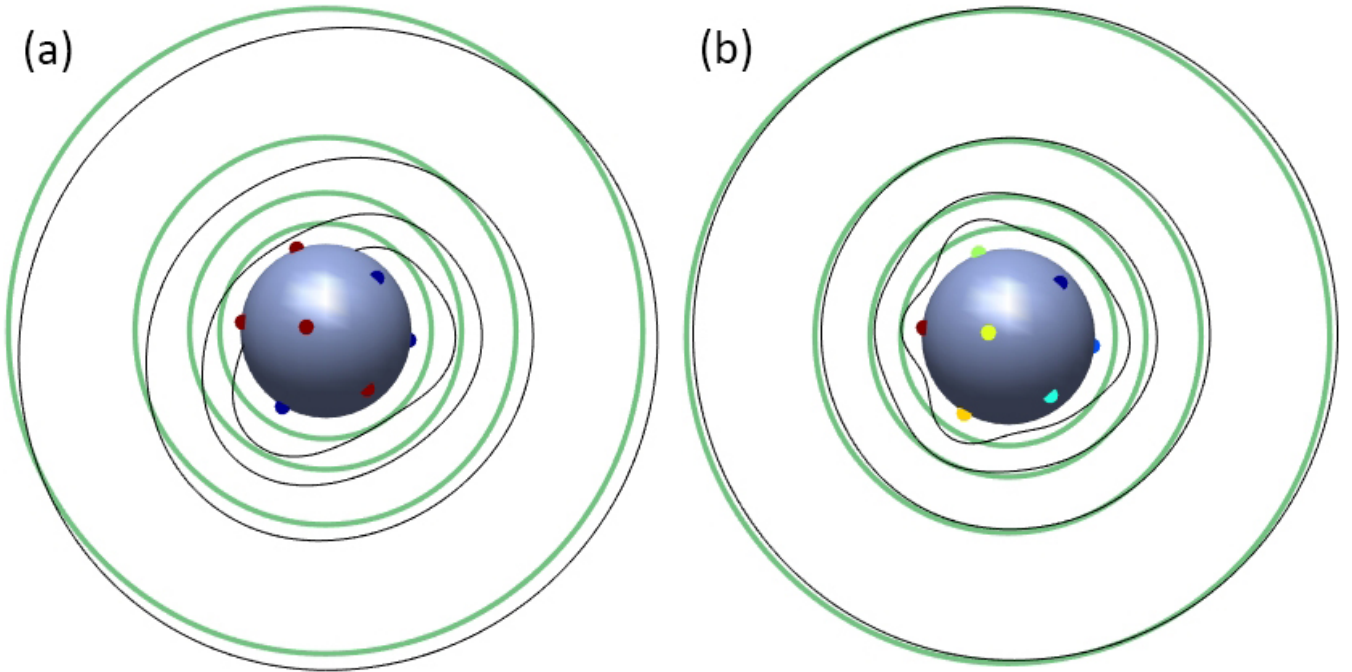

FIG. 8. Contour lines for the electrostatic potential. Green lines show the potential contours for a point charge centered at the origin, black lines show the potential contours calculated for charge located at each patch point. a) Grain charged in PPD plasma condition where the average grain charge is 4.7 e⁻. Here five of the patches, designated by the blue dots, have one electron. The patches indicated by the red dots have no charge. b) Grain charged in LAB plasma conditions with an average charge of 214 e⁻. The patch charges range from 15 e⁻ (red) to 30 e⁻ (dark blue).

Previous studies have shown that the distribution of charge over an aggregate surface changes the morphology of grains produced through collisions, primarily due to rotations of the aggregates caused by the electrostatic torques [23], [24]. Thus it is of interest to determine the effects of the fluctuating charge distribution on aggregate growth. The effect on the dynamics is determined by the relative charging timescale and the particle interaction time during collisions. If the charge fluctuation time is long compared to the interaction time, then the charge can be considered to be constant during the interaction. This was the case modeled in [12] for a PPD plasma using a model for continuous stochastic charging. However, this study did not take into account the charge distribution on spherical monomers, which were treated as point charges. If the charge fluctuation time is shorter than or comparable to the interaction time,

then the charge will continuously change as the two particles approach, altering the forces and torques acting on the two particles. This is the case for the LAB plasma conditions.

Here we examine aggregation in the two different plasma environments, modeling the growth through the addition of single spherical monomers, or particle-cluster aggregation (PCA). Three different models of charge interactions are examined and compared to the coagulation of uncharged particles, as illustrated in Figure 9:

Neutral: The aggregates are not charged.
Average: The time-averaged charge on each aggregate is used – no stochastic fluctuations are considered.
Sphere: The charge fluctuates stochastically, but only the average charge on each monomer is considered (i.e. spherical monomers are treated as point charges)
Patch: The charge fluctuates stochastically, and the surface charge on each patch is considered in calculating the forces and torques (therefore spheres will have higher-order multipole moments).
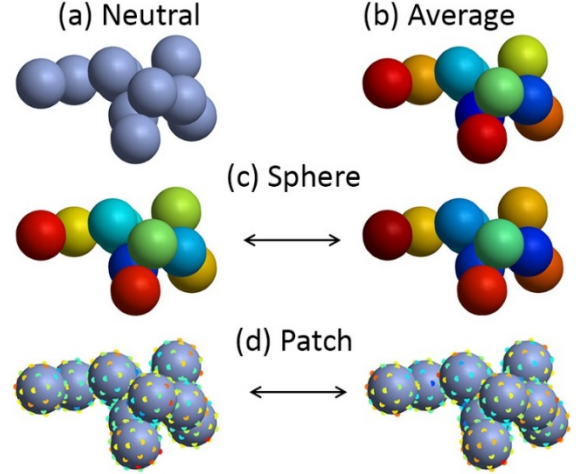

FIG. 9. (Color online) Four different charging cases considered in the aggregate dynamics. (a) All particles are uncharged, (b) the time-averaged charge is applied to each spherical monomer, (c) the total charge on each monomer fluctuates in time, (d) the charge on each patch fluctuates in time. For the spheres, red indicates a large (negative) charge and blue indicates a small (negative) charge. For the patches, red indicates the largest negative charge, and blue is the largest positive charge.

A target particle is placed with its center of mass at the origin, and an incoming particle short towards the target from a rancom direction. The average equilibrium charge on the grains is estimated for the given plasma conditions by balancing the electron and ion currents to determine the grain potential. Since we want to detect events which lead to collisions, the incoming particle is placed at a distance $D = 10(R + a)$, where R is the maximum radius of the target aggregate, as indicated in Fig. 5, and given a velocity directed towards the origin plus a random offset vector up to $(R_\sigma + a)$ in magnitude. As we are interested in detecting collisions which lead to growth, the magnitude of the incoming particle's velocity v_{Coul} is just large enough to overcome the Coulomb potential barrier at a distance $d = R_\sigma + a$, calculated using the *average* charge of each particle. Each particle is then charged employing the DSC algorithm for a sufficiently long time to cover several charge fluctuations of magnitude 1σ, such that each particle has an initial random deviation from the average charge.

In the LAB plasma, we consider 25 nm melamine formaldehyde spheres ($n = 10$ patches) with mass density $\rho = 1500$ kg/m³. The fluctuation time τ_c is on the order of 100 ns, which is comparable to the modeled interaction time $\tau_d = (D - d) / v_{coul}$. In the *Sphere* and *Patch* models, the charge is allowed to change during the interaction by calling the DSC algorithm and allowing fluctuations to occur (adding one electron or one ion each random time step) until the elapsed charging time equals the dynamic time step. In the PPD environment we model the dynamics and growth of silicate grains with mass density $\rho = 2500$ kg/m³ using monodisperse spheres with $a = 100$ nm ($n = 10$ patches). In this case, τ_c is on the order

of tenths of seconds while the interaction time τ_d is on the order of milliseconds. The charge is allowed to fluctuate with the *Sphere* and *Patch* models, but this happens infrequently as $\tau_d \ll \tau_c$.

After each collision, the charge on the new aggregate is obtained by running the DSC algorithm for a time long enough to cover several fluctuations of magnitude 1σ. A new monomer (with randomized charge) is set at a random incoming direction and shot towards the target. Aggregates are built up to 25 monomers in size, with more than 100 aggregates built for each case.

To speed up the calculations, outside of a distance of $4R$, where R is the maximum radial extent of the target particle measured from the center of mass (COM) (see Fig. 5), multipole expansions of the particles' potentials (up to the quadrupole terms) are used to calculate the electrostatic forces and torques acting on each aggregate. Inside this distance, either the charge on each monomer (*Average*, *Sphere*) or the charge on each patch (*Patch*) is used to calculate the electric fields [24].

Figures 10-12 compare the physical characteristics of the aggregates formed using the different charging cases in both plasma environments. In all three figures, the data points represent the average quantity for all aggregates with N monomers. One characteristic of particular interest for aggregate growth is porosity, or the amount of empty space, as this controls how well an aggregate couples to the gas and the surface area available for holding charge. The equivalent radius can be used to define the compactness factor Φ_σ which is the ratio of the volume of the constituent monomers to the volume of a
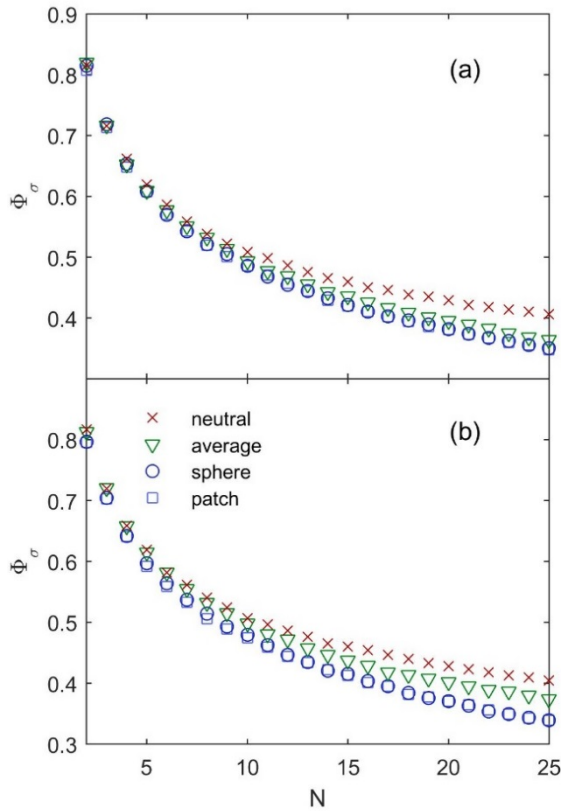

FIG. 10. Compactness factor as a function of the number of monomers for (a) LAB plasma and (b) PPD plasma.
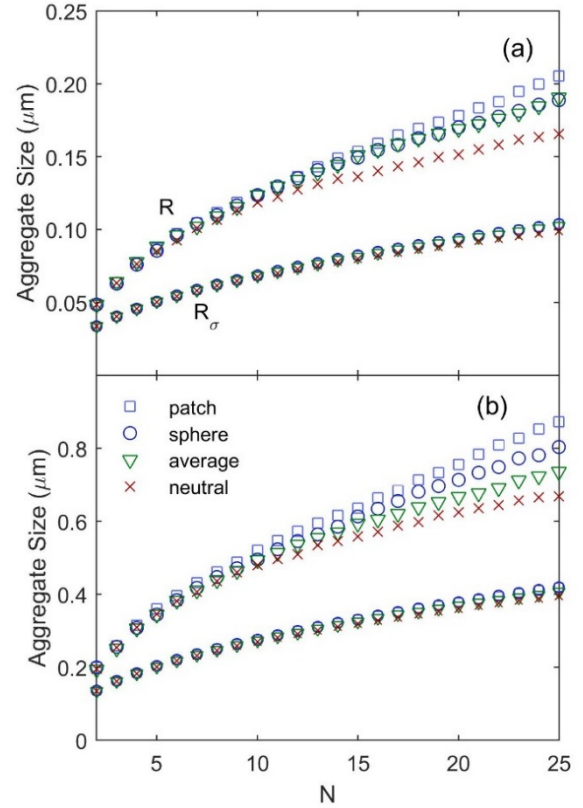

FIG. 11. Aggregate size as a function of the number of monomers N for (a) LAB plasma, (b) PPD plasma. The upper curves designate the average maximum radial extent, R, measured from the center of mass, while the lower curves show the average equivalent radius R_σ.

sphere of radius R_σ [22]. Thus a sphere has a compactness factor of one, while $\Phi_\sigma < 1$ for a fluffy, porous aggregate. As expected, charged grains are "fluffier" than uncharged grains as seen by the decreased compactness factor (Fig. 10), and the aggregates built with stochastic variations (*Patch* and *Sphere* cases) have the lowest (though indistinguishable) compactness factors. Plots of the average aggregate size as a function of the number of monomers are shown in Figure 11. Although R_σ is almost identical for each of the four cases on the scale shown, the maximum radial extent of the aggregates, R, is quite different. The differences between the different charging models are more clearly seen in plots of R_σ/R (Figure 12), which is used as a proxy for the aspect ratio of the aggregates. In both the LAB plasma and PPD plasma conditions, taking into consideration the fluctuations at each point on the surface (*Patch*) resulted in aggregates with the largest aspect ratios. It is of interest to note that in the LAB plasma, where the fluctuation time is shorter than or comparable to the dynamical timescale for the particle interaction, the difference between the time-averaged charge (*Average*) and the charge on each monomer (*Sphere*) is small.
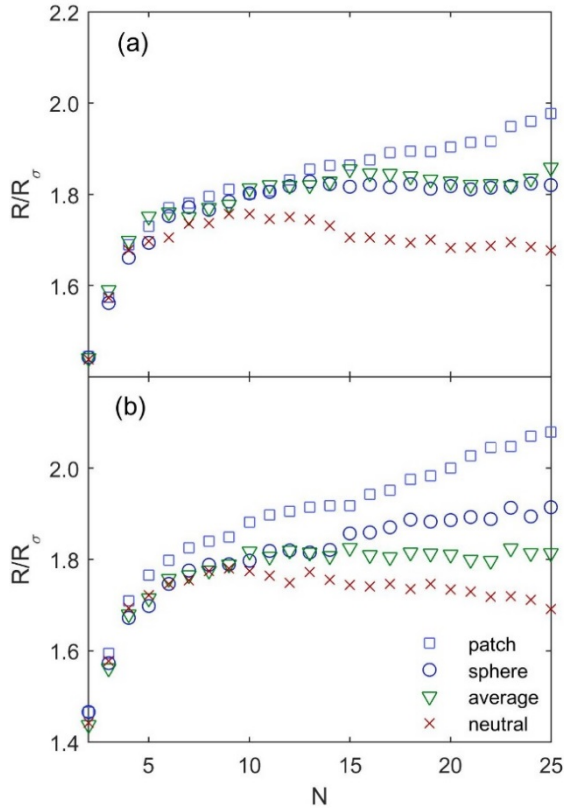

FIG. 12. Ratio of the maximum radial extent to the equivalent radius as a function of the number of monomers for (a) LAB plasma, and (b) PPD

Sample aggregates from the *Patch*, *Average*, and *Neutral* cases for the PPD plasma conditions are shown in Figure 13, which illustrates the difference in aspect ratios. Here each aggregate has been rotated so that the direction of maximum extent (as measured from the COM) lies along the x-axis. As shown, the aggregate built with the *Patch* charge variations is much more elongated (Figure 13a).

A consequence of the increased aspect ratio of the aggregates is that the incoming monomers are more likely to approach from a direction where they cannot overcome the Coulomb repulsion barrier before making contact with the target aggregate. Thus the number of interactions between grains which do not lead to collisional growth increases as the aggregates grow. The average cumulative number of misses in growing to an aggregate size of N monomers is shown in Fig. 14. The average number of missed collisions is the same for all of the charged grain models when the grains are small, but after reaching a certain size (or aspect ratio) the grains with fluctuating charges (*Patch* and *Sphere* models) are less likely to collide.
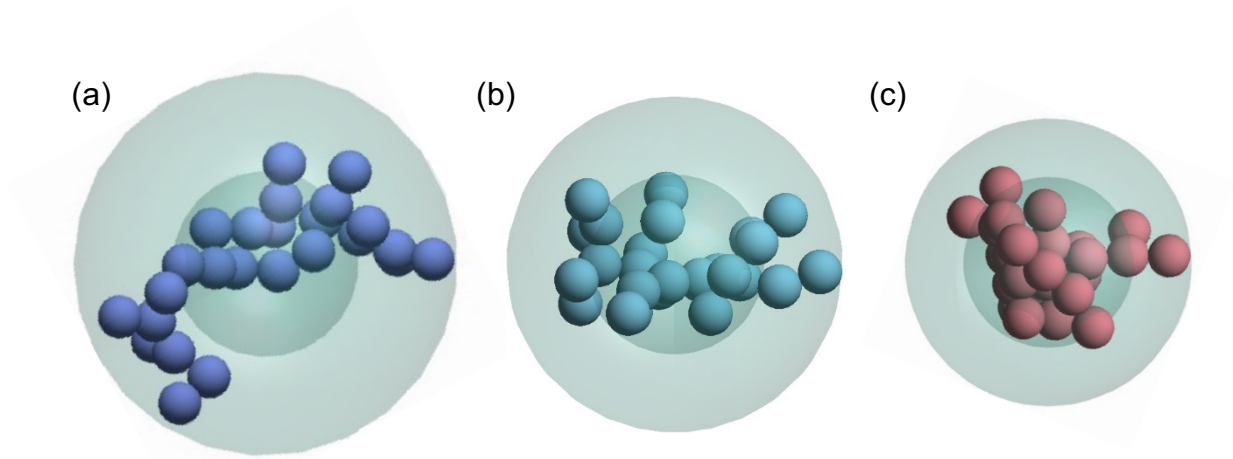
FIG. 13. Comparison of aggregates built using the different charging models in PPD plasma conditions. All aggregates have 25 monomers. a) *Patch* charge with DSC, b) constant *Average* charge, c) *Neutral*. The inner sphere shows the extent of R_σ, which is approximately equal for the three aggregates, while the outer sphere indicates the maximum radial extent.
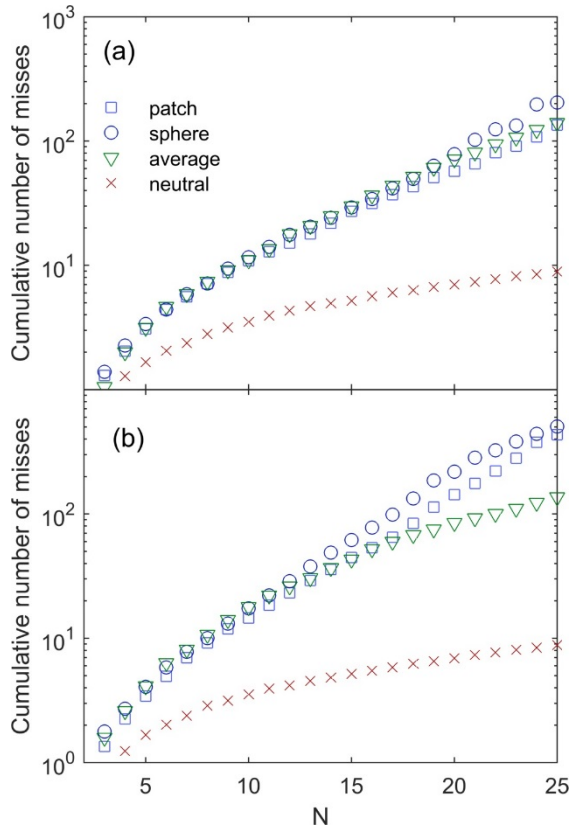

FIG. 14. Cumulative number of misses in building aggregate to N monomers for (a) LAB plasma and (b) PPD plasma.

VI. CONCLUSION AND DISCUSSION

We have presented a numerical model that allows examination of the charge fluctuations on the surface of an aggregate grain created by discrete stochastic charging and the effect these fluctuations have on the overall dynamics of the aggregation process. The discrete stochastic method (DSM) considers additions of single electrons or ions to patches on the surface of an aggregate based on calculated electron and ion currents to the surface points. The model recovers the results previously derived for spherical grains, where the sphere was treated as an isopotential surface [2]–[5]. It is shown that the mean and standard deviation of charge on aggregate grains follows the same trends as those predicted for spheres having an equivalent radius.

An underlying assumption in the DSM is that the charging currents vary linearly with the grain charge, which leads to a minimum grain size which can be accurately treated by this method [5]. Here we have applied this minimum size criterion to the patches, thus the DSM becomes less accurate as the number of patches on the surface of the grain is increased (Figure 3). However it is important to note that the accuracy of the charge calculation using OML_LOS increases as the number of patches is increased for two reasons. First, the contribution to the patch potential from the charge on a patch itself is approximated assuming the patch boundary is essentially circular. This assumption becomes less accurate as the number of patches decreases (with the exception being that it is exact for $n = 2$). Second, for aggregate grains, the maximum number of patches used must be balanced against the minimum number of patches required to resolve the LOS_factor. In order to accurately resolve the blocked lines of sight, the patch size needs to be comparable to the size of the smallest monomer (in the case of a polydisperse distribution of monomers) where in this case, $n = \left(2a_{max}/a_{min}\right)^2$. This can lead to a contradiction where $n_{min} > n_{max}$, in which case a compromise must be reached. Fortunately, the two constraints offset each other to a certain extent since using too many patches on the surface results in an over-estimation of the average charge on a particle (i.e., for a negatively charged grain, the number of electrons), while using too few patches results in the charge being underestimated, since additional LOS are blocked. The simulations presented here show that good results can be obtained for n as small as 10.

When applying the DSM to aggregate grains, the average charge on the aggregates tends to be greater than the average charge collected by spherical grains, primarily due to the increased surface area as previously reported [15], [18]. The primary difference between aggregates and spherical grains lies in the nature of the charge fluctutations, which differ two ways. The first is that the standard deviation in the charge on aggregate grains tends to be greater than that predicted for a sphere of equivalent size (Figure 6). The second is that the time scale of the fluctuations on aggregates tends to be shorter than that for a sphere of equivalent size (Figure 7). While the mean aggregate charge and its standard deviation may differ by as much as 20% from that on a spherical grain, the time scale of the fluctutations can differ by a factor of three to ten.

While it is generally accepted that the distribution of charge over the irregular surface of an aggregate grain can influence its growth process, here we show that an uneven distribution of charge on a spherical grain due to charge fluctuations (Figure 8) can also impact both the growth process and physical characteristics of the aggregates. In particular, this irregular distribution of charge tends to produce aggregates which are much more linear or filamentary (see Figures 12 and 13). This becomes most important for submicron-sized grains in environments where the charge fluctuations occur on timescales similar to the dynamical time scales. Additionally, at some point in the growth of filamentary aggregates, the collection of monomers becomes less efficient (Fig. 14), slowing the rate of growth or even halting it. The precise point at which this effect becomes important in an environment will depend on many factors

including coupling with the gas, the relative velocities between grains, other forces acting on the grains, and the number density of solid particles.

These results may partly explain the observations of recent experiments wherein ice aggregates were grown from water vapor injected in an RF discharge. The aggregates vary in both size and aspect ratio as the background gas pressure and type of gas is varied, having greater aspect ratios in lighter-mass gases and lower gas pressures [25], [26]. Both of these observations may be partly explained by the charge fluctuations occurring on the surface of the smallest ice droplets as they condense out of the vapor. As the ion mass increases, the average charge on the grains increases, resulting in smaller charge fluctuations. Such smaller fluctuations mean that the dynamics will be more similar to those observed for the *Sphere* or *Average* cases, resulting in less linear aggregates. As seen in Eq. 13, the fluctuation timescale is inversely proportional to the plasma density. Thus, as the pressure is decreased, the fluctuation timescale increases, allowing the fluctuations to have greater influence on the dynamics, as seen in the *Patch* case, which formed elongated aggregates. Of course, it should be noted that the aggregates in these experiments were formed in and aligned with a vertical electric field, which is required to levitate the grains against gravity. Thus collisions may occur along a preferred direction, increasing the overall linearity of the aggregates.

The morphology of grains can have important implications in in many astrophysical environments. Most simulations which include the effects of dust in protoplanetary disks assume the dust to be spherical particles, though the polarization of sunlight from cometary dust (comets being the most primitive bodies in the solar system) suggests the presence of dust particles with ellipsoidal shapes and aspect ratios of 3:1 [27]. The shape and porosity of grains determine the coupling of the grains with the gas, affecting the rate of growth of the aggregates [28]–[30]. In turn, aggregate dust grains absorb charged particles more efficiently than solid spheres, affecting the degree of ionization of gases in protoplanetary disks. The ionization levels affect the coupling of magnetic fields to the disk gas, and as the turbulent gas flows drive the collisional growth of grains, the charge on the grains is an important feedback mechanism in disk processes [31]–[33]. Another area of interest is the dust in the interstellar medium (ISM). It has long been recognized that the polarization of light passing through the ISM indicates that the dust grains are elongated with their long axes aligned perpendicular to the magnetic field [34]. Measurements in frequency bands dedicated to Cosmic Microwave Background studies have also shown strong evidence for a grain alignment mechanism throughout the ISM [35]. Charging of grains by photoemission is the main source of heating in the interstellar medium (ISM) (see [36] and the references therein), so a description of charging of irregular small particles could have profound implication for our understanding of the dynamical evolution of the ISM.

REFERENCES

[1]   Morfill, G. E., E. Grün, & T. V. Johnson, Planet. Space Sci. 28, 1087 (1980).
[2]   Draine, B. T. and B. Sutin, Astrophys J, 320, 803 (1987).
[3]   Cui, C. and J. Goree, IEEE Trans. Plasma Sci. 22, 151 (1994).
[4]   Matsoukas, T. and M. Russell, J. Appl. Phys. 77, 4285 (1995).
[5]   Matsoukas, T. and M. Russell, Phys. Rev. E 55, 991 (1997).
[6]   Shotorban, B., Phys. Rev. E 83, 066403 (2011).

[7]   Shotorban, B., Phys. Plasmas 19, 053702-053702-6 (2012).

[8]   Selwyn, G. S., J. Singh, and R. S. Bennett, J. Vac. Sci. Technol. Vac. Surf. Films 7, 2758 (1989).

[9]   Boufendi, L. and A. Bouchoule, Plasma Sources Sci. Technol. 3, 262 (1994).

[10] Chai, K.-B. and P. M. Bellan, Geophys. Res. Lett. 40, 2013GL058268 (2013).

[11] Sayes, C. M. et al., Inhal. Toxicol. 22, 348 (2010).

[12] Matthews, L., B. Shotorban, and T. W. Hyde, Astrophys. J. 776, 103 (2013).

[13] Matthews, L. S. and T. W. Hyde, IEEE Trans. Plasma Sci. 32, 586 (2004).

[14] Ivlev, A. V., G. E. Morfill, and U. Konopka, U. Phys. Rev. Lett. 89, 195502 (2002).

[15] Ma, Q., L. S. Matthews, V. Land, and T. W. Hyde, Astrophys. J. 763, 77 (2013).

[16] Allen, J. E., Probe theory - the orbital motion approach. Phys. Scr. 45, 497 (1992).

[17] Laframboise, J. G. and L. W. Parker, Phys. Fluids 16, 629 (1973).

[18] Matthews, L. S., V. Land, and T. W. Hyde, Astrophys. J. 744, 8 (2012).

[19] Van Kampen, N. G., Stochastic Processes in Physics and Chemistry. (Elsevier, Amsterdam, 2007).

[20] Gillespie, D. T., J. Comput. Phys. 22, 403 (1976).

[21] Gillespie, D. T., Annu. Rev. Phys. Chem. 58, 35 (2007).

[22] Paszun, D. and C. Dominik, Astron. Astrophys. 507, 1023 (2009).

[23] Matthews, L. S. and T. W. Hyde, New J. Phys. 11, 063030 (2009).

[24] Matthews, L. S., D. A. Coleman, and T. W. Hyde, IEEE Trans. Plasma Sci. 44, 519 (2016).

[25] Chai, K.-B. and P. M. Bellan, Astrophys. J. 802, 112 (2015).

[26] Chai, K. B., IEEE Trans. Plasma Sci. PP, 1 (2017).

[27] Greenberg, J. M. and J. I. Hage, Astrophys. J., 361, 260, (1990).

[28] Ormel, C. W., M. Spaans, and A. G. G. M. Tielens, Astron. Astrophys, 461, 18 (2007).

[29] Gunkelmann, N., C. Ringl, and H. M. Urbassek, Astron. Astrophys., 589, A30, (2016).

[30] Okuzumi, S., H. Tanaka, and M. Sakagami, Astrophys. J., 707, 1247, (2009).

[31] Simon, J. B., X.-N. Bai, K. M. Flaherty, and A. M. Hughes, ArXiv171104770 Astro-Ph, (2017).

[32] Turner, N. J., S. Fromang, C. Gammie, et al., *Protostars and Planets VI*, eds. H. Beuther, R. S. Klessen, C. P. Dullemond, and T. K. Henning, University of Arizona Press, (2014).

[33] Okuzumi, S., Astrophys. J., 698, 1122 (2009).

[34] Davis, L. and J. L. Greenstein, *Astrophys. J.*, 114, 206, (1951).

[35] Benoît, A., *et al*., *Astron. Astrophys*., 424, 2, 571–582, (2004).

[36] Weingartner, J. C. and B. T. Draine, Astrophys. J. Suppl. Ser., 134, 263, (2001).